AIAA JOURNAL
Vol. 30, No. 4, April 1992

Modeling Supersonic Combustion Using a Fully Implicit Numerical Method

Gregory J. Wilson* and Robert W. MacCormack†
Stanford University, Stanford, California 94305

A fully implicit, finite volume algorithm for two-dimensional axisymmetric flows has been coupled to a detailed hydrogen-air reaction mechanism (13 species and 33 reactions) so that supersonic combustion phenomena may be investigated. Numerical computations are compared with ballistic-range shadowgraphs of a blunt body as it passes through a premixed stoichiometric hydrogen-air mixture at Mach 5.11 and 6.46. The suitability of the numerical procedure for simulating these flows is shown. The requirements for the physical formulation and the numerical modeling of these flowfields are discussed. Finally, the sensitivity of these external flowfields to changes in certain key reaction rate constants is examined, and the contributions that ballistic-range data can make toward verification of a chemical reaction mechanism is demonstrated.

Nomenclature

$c_{v_{trans}}$ = translational specific heat at constant volume
$c_{v_{rot}}$ = rotational specific heat at constant volume
E = total energy per unit volume
E_v = vibrational energy per unit volume
F,G = vector of inviscid fluxes
h° = heat of formation
K_b = backward rate coefficient
K_{eq} = equilibrium rate coefficient
K_f = forward rate coefficient
M_i = molecular weight of species i
p = pressure, $\sum_{i=1}^{ns} (\rho_i/M_i)\, RT$
R = universal gas constant
T = translational temperature
T_v = vibrational temperature
U = vector of conserved variables
u,v = Cartesian velocities in the x and y directions, respectively
W = vector of source terms
w_i = chemical source term in species equation i
w_v = vibrational energy equation source term
x,y = Cartesian coordinates
ρ = total density, $\sum_{i=1}^{ns} \rho_i$

Subscripts
i = species i
j = reaction j
nm = number of polyatomic species
ns = number of species

Introduction

THE motivation for investigating supersonic flows with hydrogen-air combustion comes from a need to understand the flow through supersonic combustion engines and through experimental facilities that use combustion processes in their operation, such as shock tunnels. Numerically simulating these flowfields is a difficult task. In addition to shock waves, viscous layers, and mixing, they include complicated combustion kinetics, diffusion processes, and large energy releases into the flowfield. Furthermore, since the fluid flow is fast (i.e., supersonic), the fluid time scales can be similar to the chemical time scales, especially at low densities where chemical reactions proceed slower. This means that chemical nonequilibrium phenomena should be included in any modeling attempt and that thermal nonequilibrium phenomena should be considered.

In this work, a numerical method that has been applied successfully to thermochemical nonequilibrium air calculations[1-5] is applied to combustion physics. To test its suitability in this new application, we simulate the flow over a blunt body passing through a premixed hydrogen-air mixture and compare the simulations to the experiments of Lehr[6] (Figs. 1 and 2). These particular flowfields provide an excellent example of the complicated flow physics that can exist in supersonic flows with combustion. Their most notable feature is a double-front phenomenon resulting from a coupling of the fluid dynamics and nonequilibrium chemical kinetics. The ability to simulate such flows provides a convincing validation of a combined numerical method and combustion mechanism. This is supported by a recent paper by Candler[4] who shows that experimental data for shock shapes and shock positions are very useful for code validation in chemically reacting air. When a numerical model properly reproduces macroscopic quantities like the shock-standoff distance, this is evidence that the gas model is predicting the proper degree of reaction and thermal excitation.

Several researchers[7,8] have recently attempted to simulate Lehr's ballistic-range data but were unable to calculate the correct shock-standoff distance and reaction front location for the test at Mach 6.46. These authors discuss possible reasons for the differences they see between their calculations and the experiments. These discussions question whether certain chemical species need to be included in the reaction mechanism, and/or whether reaction rates are known accurately enough, and/or whether thermal nonequilibrium effects need to be taken into account, and whether special numerical techniques need to be used. This paper attempts to address these questions.

One simplifying aspect of using Lehr's experiments is that the flowfield physics are predominantly driven by reaction kinetics and convection phenomena. This means that the complications and uncertainties that diffusion and mixing can introduce are small or even removed from the problem. As a result, differences between the experimental data and numerical calculations are attributed either to numerical errors or to

Presented as Paper 90-2307 at the AIAA/SAE/ASME/ASEE 26th Joint Propulsion Conference, Orlando, FL, July 16–18, 1990; received Aug. 13, 1990; revision received May 1, 1991; accepted for publication May 7, 1991.

*Graduate Student, Department of Aeronautics and Astronautics. Student Member AIAA.

†Professor, Department of Aeronautics and Astronautics. Member AIAA.

improperly modeled chemical kinetics. It is hoped that if the numerical errors can be understood, then this work may provide a tool for refining the reaction mechanism for the hydrogen-air combustion. The utility of these flowfields for refining reaction mechanisms is tested by altering several key reaction rate constants and noting the resulting changes to the flowfields.

Governing Equations

The Euler equations are used since viscous and diffusion effects are believed to be small. To provide the capability to study vibrational nonequilibrium there are two energy equations; one for the total energy and one for the vibrational energy. With the inclusion of ns species equations and two momentum equations, the resulting formulation contains $ns + 4$ coupled equations. The formulation written in conservation law form for two dimensions in Cartesian coordinates is

$$\frac{\partial U}{\partial t} + \frac{\partial F}{\partial x} + \frac{\partial G}{\partial y} = W \tag{1}$$

where the state vector, the source vector, and the convective flux vectors are defined as follows:

$$U = \begin{pmatrix} \rho_1 \\ \rho_2 \\ \vdots \\ \rho_{ns} \\ \rho u \\ \rho v \\ E_v \\ E \end{pmatrix}, \quad W = \begin{pmatrix} w_1 \\ w_2 \\ \vdots \\ w_{ns} \\ 0 \\ 0 \\ w_v \\ 0 \end{pmatrix}$$

$$F = \begin{pmatrix} \rho_1 u \\ \rho_2 u \\ \vdots \\ \rho_{ns} u \\ \rho u^2 + p \\ \rho uv \\ uE_v \\ u(E + p) \end{pmatrix}, \quad G = \begin{pmatrix} \rho_1 v \\ \rho_2 v \\ \vdots \\ \rho_{ns} v \\ \rho uv \\ \rho v^2 + p \\ vE_v \\ v(E + p) \end{pmatrix} \tag{2}$$

The total energy is written as

$$E = \sum_{i=1}^{ns} \rho(c_{v_{\text{trans}i}} + c_{v_{\text{rot}i}})T + E_v + \frac{1}{2}\rho(u^2 + v^2) + \sum_{i=1}^{ns} \rho_i h_i^\circ \tag{3a}$$

where

$$E_v = \sum_{i=1}^{nm} E_{v_i} \tag{3b}$$

In Eq. (3a), the first term represents the translational and rotational energies per unit volume. The second term E_v represents the vibrational energy per unit volume, and the last two terms are the kinetic energy and the chemical energy per unit volume.

Equation (3b) defines the total vibrational energy per unit volume as the sum of the vibrational energies for each species with internal structure. There are nm of these species. All of the nm species are considered to be harmonic oscillators and are considered to be at a single vibrational temperature T_v. Equation (3b) is used to solve for vibrational temperature T_v. An advantage of this formulation is that curve-fit tables are not needed to obtain the internal energy. Instead only the heats of formation and the characteristic vibrational temperatures are required as inputs and then the internal energy can be calculated. The thermodynamic data are from the JANAF tables[9] with the exception of the characteristic vibrational temperatures for hydrogen peroxide, which were taken from a recent paper by Willetts et al.[10]

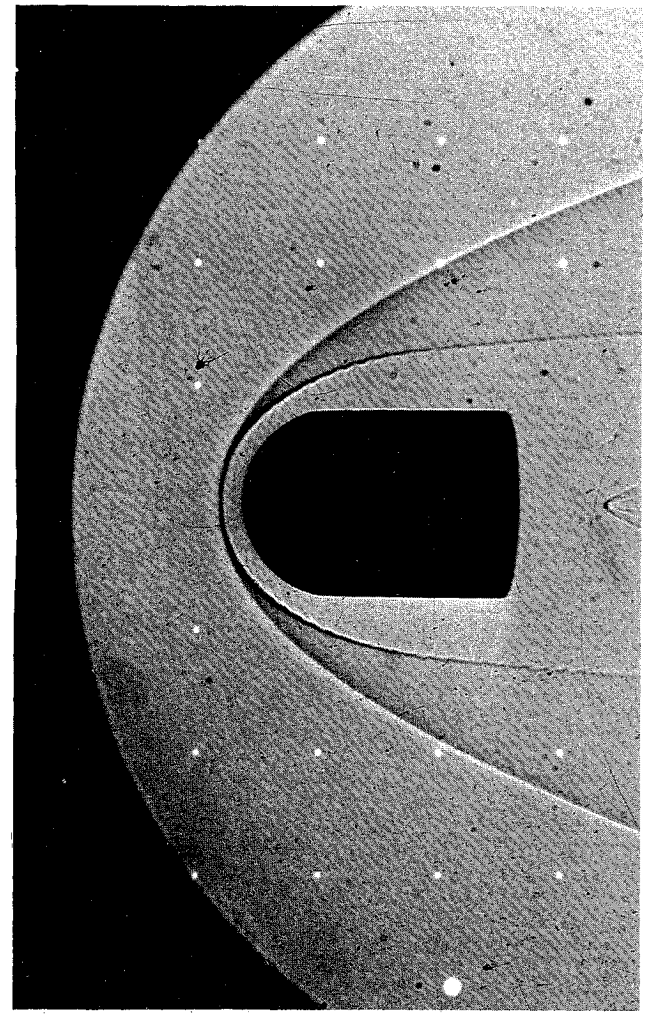

Fig. 1 Shadowgraph of a spherical nose projectile moving at Mach 5.11 in a hydrogen-air mixture.

The vibrational source term is in the form of Laudau-Teller relaxation. It is not considered important in this work because good agreement with experimental data is achieved with very fast relaxation rates so that the gas is essentially in thermal equilibrium, i.e., $T_v = T$.

Chemistry Model

The hydrogen-air combustion mechanism used in this work is based on the detailed mechanism proposed by Jachimowski,[11] which consists of 13 reaction species (N_2, O_2, H_2, NO, OH, NO_2, HNO, HO_2, H_2O, H_2O_2, N, O, H) and 33 reactions. This particular mechanism is used because it is detailed, well documented, and refined to match experimental data. It includes all of the important species in the hydrogen-oxygen system and includes reactions for the species N, NO, and HNO which may become important at higher Mach number conditions in scramjet applications. The reaction set is presented in Table 1. Note that it is slightly different than the mechanism in Ref. 11. Reaction (1) in Ref. 11,

$$(1) \quad H_2 + O_2 \rightleftharpoons OH + OH$$

is replaced by Reaction (1′)

$$(1') \quad H_2 + O_2 \rightleftharpoons H + HO_2$$

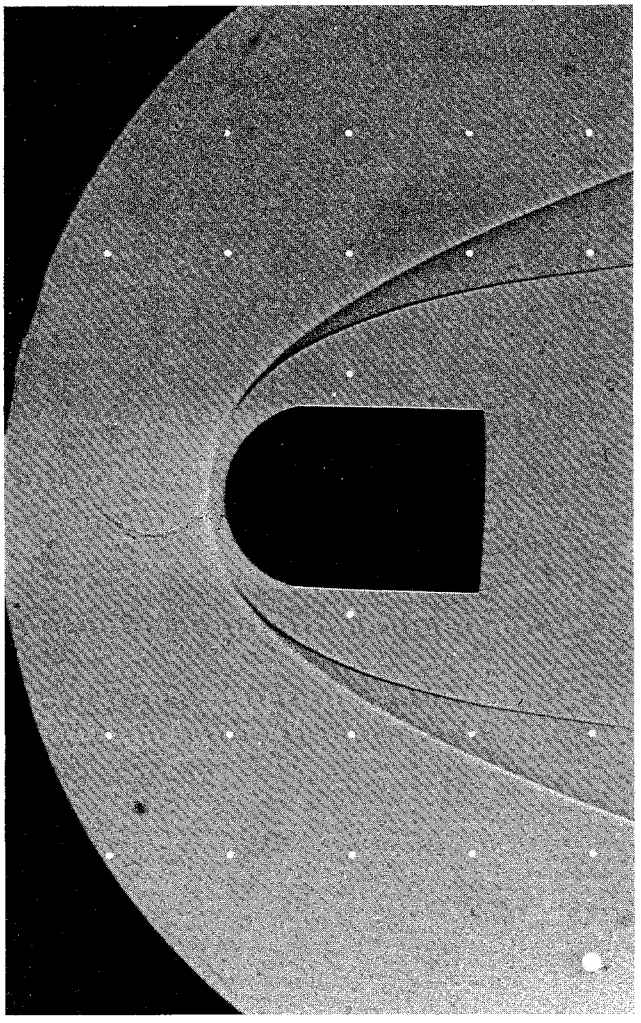

Fig. 2 Shadowgraph of a spherical nose projectile moving at Mach 6.46 in a hydrogen-air mixture.

and Reaction (10) is omitted because it is the reverse of the new Reaction (1′). These changes are recommended by Oldenborg et al.[12] because it is unlikely that the collision of H_2 and O_2 will lead directly to OH formation. The rate constant for Reaction (1′) is different from the original expression, as well.

The forward rate constants are found in Table 1. The backward rate constants are calculated using the equilibrium constant for each reaction and the relation

$$K_{eqj} = \frac{K_{fj}}{K_{bj}} \tag{4}$$

The equilibrium constants are calculated from the standard Gibbs free energy difference for each reaction. This calculation requires the standard Gibbs free energy for each species. These values were obtained using the NASA polynomials for enthalphy and entropy taken from the Appendix of Ref. 13.

There is uncertainty in applying the reaction mechanism in Table 1 to the ballistic-range experiments because the pressures and temperatures found behind the projectile bow shocks are outside the conditions for which the mechanism was validated. The data used by Jachimowski to validate ignition delay times are mostly between pressures of 0.5 and 2 atm and temperatures between 800 and 1500 K, whereas the conditions behind a Mach 6 bow shock in the ballistic range are over 17 atm and 2300 K. Therefore, it is reasonable to expect that some refinement of the reaction rates may be necessary to improve the comparisons with experiment at new conditions. In this paper, refinements are limited to Reactions (2) and (6) for simplicity. This limitation has added value because each of these two reactions has a strong but different influence on combustion calculations. The differences between the two are discussed in the following.

It is well known that Reactions (2) and (9)

$$(2)\ H + O_2 \rightleftharpoons OH + O$$

$$(9)\ H + O_2 + M \rightleftharpoons HO_2 + M$$

are very influential in determining ignition delay times. Reaction (2) is the primary chain branching reaction and Reaction (9) is the primary source of HO_2. At lower temperatures (below 1500 K), these two reactions compete and greatly influence the amount of the OH radical being produced. Small changes in these two rates can have a large affect on the mechanism properties. The reason that changes are confined to Reaction (2) in this work, rather than to both Reactions (2) and (9), is that Reaction (9) becomes less important in the induction zone at high temperatures. Changing the rate constant to Reaction (2) is sufficient to modify the ignition delay time and reveal the flowfield sensitivity to this effect. This does not mean that the HO_2 reactions are negligible at high temperatures. In fact, a major point of Jachimowski's paper was to establish the importance of including HO_2 in the hydrogen-air combustion mechanism (see Ref. 11 for more discussion).

The other rate expression altered in this paper is Reaction (6)

$$(6)\ H + OH + M \rightleftharpoons H_2O + M$$

Reaction (6) is a primary recombination reaction and the reaction that releases much of the heat during combustion. Therefore, changes to it can affect a flowfield by changing the rate at which heat is released into the flowfield, i.e., it changes the reaction time.[14] This is a different effect than changing the ignition delay time. The ignition delay time is a measure of when ignition begins, whereas the reaction time is a measure of the time needed to reach the postcombustion temperature after ignition has occurred. Note that prescribing the rate constant for Reaction (6) is complicated by the need for separate constants for the various possible third body collision partners.

Numerical Method

The numerical method is a finite volume, fully implicit, flux-split technique based on the work of MacCormack[1] and extended to real gases in thermochemical nonequilibrium by Candler.[3] It is time dependent and uses Gauss-Siedel line relaxation. The flux splitting is second-order accurate in space. First-order Steger-Warming flux splitting is used in regions of high pressure gradients, such as shocks, to maintain numerical stability. The reader is referred to Refs. 2 and 4 for a detailed description.

The fully implicit approach has proven to be efficient in previous nonequilibrium flow calculations[3,5] and it is attractive for combustion problems because the chemistry time scales can cause the equation set to be extremely stiff. The costs of using this approach are expensive time steps, large memory requirements, and complicated coding. The advantage in using the implicit approach is that large time steps are permitted, which, in turn, allows a steady-state solution to be reached quickly.

Adaptive Grid

The adaptive grid technique adopted for this work is based on the scheme used by Gökçen.[5] The grid dynamically moves each time step so that evolving physical phenomenon are resolved accurately. The clustering of points is achieved by requiring that the product of the grid spacing and a weight function is constant throughout the mesh. According to this constraint, where the weight function is large, grid spacing is

Table 1 Jachimowski's H_2/Air combustion mechanism[a,b]

j	Reaction[c] j	A_j	n_j	E_j
(1′)	$H_2 + O_2 \rightleftharpoons HO_2 + H$	1.00×10^{14}	0	56,000
(2)	$H + O_2 \rightleftharpoons OH + O$	2.60×10^{14}	0	16,800
(3)	$O + H_2 \rightleftharpoons OH + H$	1.80×10^{10}	1.00	8,900
(4)	$OH + H_2 \rightleftharpoons H_2O + H$	2.20×10^{13}	0	5,150
(5)	$OH + OH \rightleftharpoons H_2O + O$	6.30×10^{12}	0	1,090
(6)	$H + OH + M \rightleftharpoons H_2O + M$	2.20×10^{22}	−2.00	0
(7)	$H + H + M \rightleftharpoons H_2 + M$	6.40×10^{17}	−1.00	0
(8)	$H + O + M \rightleftharpoons OH + M$	6.00×10^{16}	−0.6	0
(9)	$H + O_2 + M \rightleftharpoons HO_2 + M$	2.10×10^{15}	0	−1,000
(10)	omitted	—	—	—
(11)	$HO_2 + H \rightleftharpoons OH + OH$	1.40×10^{14}	0	1,080
(12)	$HO_2 + H \rightleftharpoons H_2O + O$	1.00×10^{13}	0	1,080
(13)	$HO_2 + O \rightleftharpoons O_2 + OH$	1.50×10^{13}	0	950
(14)	$HO_2 + OH \rightleftharpoons H_2O + O_2$	8.00×10^{12}	0	0
(15)	$HO_2 + HO_2 \rightleftharpoons H_2O_2 + O_2$	2.00×10^{12}	0	0
(16)	$H + H_2O_2 \rightleftharpoons H_2 + HO_2$	1.40×10^{12}	0	3,600
(17)	$O + H_2O_2 \rightleftharpoons OH + HO_2$	1.40×10^{13}	0	6,400
(18)	$OH + H_2O_2 \rightleftharpoons H_2O + HO_2$	6.10×10^{12}	0	1,430
(19)	$M + H_2O_2 \rightleftharpoons OH + OH + M$	1.20×10^{17}	0	45,500
(20)	$O + O + M \rightleftharpoons O_2 + M$	6.00×10^{13}	0	−1,800
(21)	$N + N + M \rightleftharpoons N_2 + M$	2.80×10^{17}	−0.75	0
(22)	$N + O_2 \rightleftharpoons NO + O$	6.40×10^{19}	1.00	6,300
(23)	$N + NO \rightleftharpoons N_2 + O$	1.60×10^{13}	0	0
(24)	$N + OH \rightleftharpoons NO + H$	6.30×10^{11}	0.50	0
(25)	$H + NO + M \rightleftharpoons HNO + M$	5.40×10^{15}	0	−600
(26)	$H + HNO \rightleftharpoons NO + H_2$	4.80×10^{12}	0	0
(27)	$O + HNO \rightleftharpoons NO + OH$	5.00×10^{11}	0.50	0
(28)	$OH + HNO \rightleftharpoons NO + H_2O$	3.60×10^{13}	0	0
(29)	$HO_2 + HNO \rightleftharpoons NO + H_2O_2$	2.00×10^{12}	0	0
(30)	$HO_2 + NO \rightleftharpoons NO_2 + OH$	3.40×10^{12}	0	−260
(31)	$H + NO_2 \rightleftharpoons NO + OH$	3.50×10^{14}	0	1,500
(32)	$O + NO_2 \rightleftharpoons NO + O_2$	1.00×10^{13}	0	600
(33)	$M + NO_2 \rightleftharpoons NO + O + M$	1.16×10^{16}	0	66,000

[a]Reactions (1) and (10) differ from Ref. 11 mechanism due to corespondence with Jachimowski.
[b]$K_{fj} = A_j T^{n_j} e^{-E_j/RT}$; units are in seconds, moles, cubic centimeters, calories, and Kelvin.
[c]Third body efficiencies relative to N_2:
Reaction (6) H_2O = 6.0
Reaction (7) H_2O = 6.0; H_2 = 2.0
Reaction (8) H_2O = 5.0
Reaction (9) H_2O = 16.0; H_2 = 2.0
Reaction (19) H_2O = 15.0

small and where the weight function is small, grid spacing is large. The weight function is defined in such a way that it increases in magnitude where there are flowfield gradients. Thus, points are concentrated in high gradient areas. For the two-dimensional calculations presented later, this adaptation scheme is applied separately along each of the grid lines leaving normal to the body (referred to as the normal direction). Since the adaptations proceed independently on each of these normal lines, a smoothing procedure is used to couple adjacent lines (referred to as the axial direction).

The weight function used in this work is based on changes in the following six different quantities: density, pressure, temperature, OH mole fraction, logarithm of the OH mole fraction, and the derivative of OH mole fraction. A combination of different quantities are used because in some regions one quantity may have large gradients whereas another may not. For example, the OH quantities have large gradients in the induction zone where quantities such as pressure and temperature are nearly constant.

Experimental Data

The ballistic-range shadowgraphs of Lehr[6] at Mach 5.11 and 6.46 are shown in Figs. 1 and 2, respectively. Both have a freestream with a temperature of 292 K, a pressure of 320-mm Hg, and both contain premixed stoichiometric hydrogen-air. At first glance, it appears that there are two shock waves produced by the body. The outer discontinuity is, in fact, a bow shock ahead of the body, but the second is an energy-release reaction front (referred to as the reaction front) produced by the ignition of the heated mixture behind the bow shock. The separation between the shock front and the reaction front is called an induction zone. It exists because the ignition kinetics have a time scale similar to the fluid time scales. This means that even though a fluid particle begins the ignition process in the chemical reactions occurring just behind the shock, it has time to travel downstream before the energy release of ignition occurs. In general, the ignition time (and the separation between the two fronts) decreases with increasing temperature because the chemical reactions proceed faster with increasing temperature. It follows that the separation between the shock and reaction front is smallest near the stagnation streamline where the temperature jump across the shock is largest (it is normal to the flow). The induction zone becomes larger as the shock curves around the body and becomes oblique. At some point, the bow shock becomes so oblique that the jump in the temperature across it is insufficient to ignite the mixture.

Besides being a function of the shock shape, the induction zone is also a strong function of the freestream conditions. Therefore, the flowfield can look quite different under various test conditions. For example, compare the differences between Figs. 1 and 2 where only the freestream Mach number is different for the two cases. Unsteady flow phenomena can occur when the freestream velocity is below the detonation wave speed.[6] The projectile in Fig. 1 is at the detonation wave speed, and the projectile in Fig. 2 is significantly above it at Mach 6.46.

An interesting feature of these two-front flowfields can be seen by examining the shadowgraph as one crosses the fronts. Note that the shift from light to dark across the bow shock

corresponds to the density increase across the shock. In contrast, note that the shift across the reaction front is from dark to light, indicating a drop in density. This is because there is a large temperature increase across the reaction front as energy is released and because the pressure remains nearly constant across it; therefore, the density must decrease according to the equation of state. It is evident that shock and reaction fronts are very different in nature.

Quasi-One-Dimensional Grid Study

The quasi-one-dimensional calculations presented in this section are used to investigate the grid spacing requirements for flowfields with shock-induced combustion. They will also be used to demonstrate the advantages of the adaptive grid. Note that the same chemistry model and the same second-order numerical method that are used in these quasi-one-dimensional calculations as are used in the axisymmetric calculations.

We consider supersonic flow through the converging-diverging nozzle in Fig. 3. Conditions are set so that the throat remains supersonic and a normal shock develops in the diverging portion of the nozzle (the exit flow is subsonic). The incoming flow is a premixed stoichiometric mixture of hydrogen and air and the conditions are such that there is a Mach number of 5.53, a pressure of 0.442 MPa, and a temperature of 317 K upstream of the shock. These conditions are similar to those in the ballistic-range experiments. The length of the nozzle, 0.1 cm, is also similar to the bow shock standoff distance, 0.2 cm, seen in the ballistic range. Therefore, the time and length scales for the shock-induced combustion seen in this example problem should be similar to those in the ballistic-range experiments.

The initial quasi-one-dimensional nozzle calculations are done using a series of progressively finer, equally spaced meshes. The different mesh dimensions are 32, 64, 128, 256, and 512 points. Figure 4 contains temperature profiles along the nozzle for the 32- and 64-point cases. The temperature rise behind the shock is 2000 K followed by an immediate additional rise in temperature as the combustion takes place. Figure 5 shows the 64-point solution again but also adds the 128-, 256-, and 512-point calculations. The region downstream of the shock is significantly altered by using more points. The point of Fig.

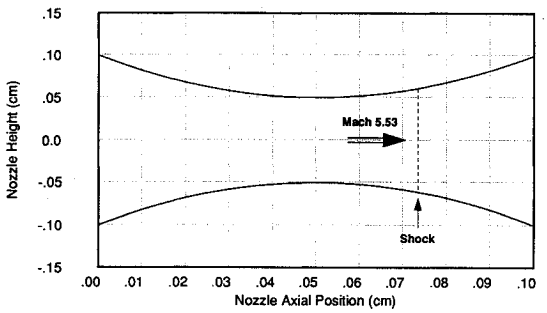

Fig. 3 Quasi-one-dimensional nozzle geometry.

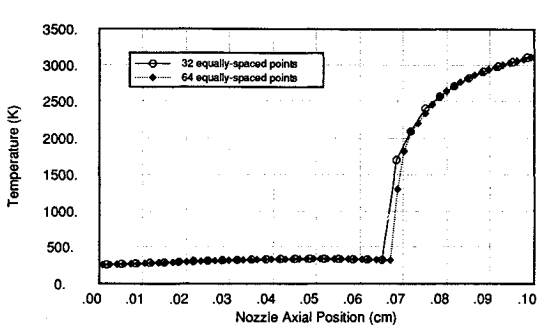

Fig. 4 Temperature profiles with an equally spaced mesh (32 and 64 points) in the quasi-one-dimensional nozzle.

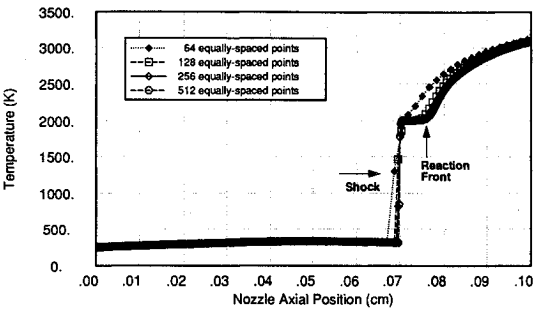

Fig. 5 Temperature profiles with an equally spaced mesh (64, 128, 256, and 512 points).

4 is that one grid refinement does not, by itself, indicate the degree that the flow is inadequately resolved. Assuming that the proper solution is captured in Fig. 5, it is concluded that it requires approximately 256 equally spaced points in the nozzle to resolve the induction zone properly with the second-order scheme.

These results show that a very large number of equally spaced grid points are required for accurate solutions. In fact, so many points are required that two-dimensional calculations would be prohibitive. This is the reason that an adaptive grid technique has been included in the present work. Fortunately, the adaptive grid approach allows the flow calculation in Fig. 5 to be done accurately with only 64 points in the nozzle and gives promise that two-dimensional calculations can be done economically.

Comparisons to Experiment and Discussion

Axisymmetric simulations of the ballistic-range experiments are now presented. Because of symmetry in the flowfield, only half the flowfield is actually calculated; however, the solutions are reflected around the symmetry line for presentation. Doing this allows a better comparison to the ballistic-range data because the projectile flowfields are not exactly symmetric (the projectiles can acquire a small angle of attack during flight). A density contour plot for a calculation simulating Lehr's Mach 5.11 case is presented in Fig. 6a. It was determined using Jachimowski's[11] recommended reaction mechanism (which will be referred to as the baseline mechanism). The symbols in the figure represent the shock and reaction front locations from the experimental shadowgraph. Figure 6b contains the 126 × 65 (65 normal) adaptive grid (reflected around the symmetry line) used for the simulation. The computation sharply captures the major features of flowfield, including the expected density drop at the reaction front. The positions of the shock and reaction fronts are relatively close to the experimental locations. Because the flowfield conditions are in a regime where the reaction mechanism is not validated, the comparison is considered good. The calculation does, however, show a larger shock-standoff distance and a smaller induction zone than is seen in the experiment.

Three possible approaches to account for the differences between the computation and the experiment will be investigated. All assume that the grid resolution is sufficient to capture accurately the solutions. The first approach attempts to reach agreement with experiment by changing the ignition delay time though modifying the rate constant for Reaction (2). The second approach assumes that the ignition delay time is correct and attempts to match experiment by changing only the reaction time, or rate of combustion. This is done by altering Reaction (6). The third approach investigates the effect of water vapor in the freestream. Water vapor can inhibit ignition and could explain the differences between the experiment and the calculations.

Consider the first of these approaches, modifying the ignition delay. To achieve better agreement with the experiment,

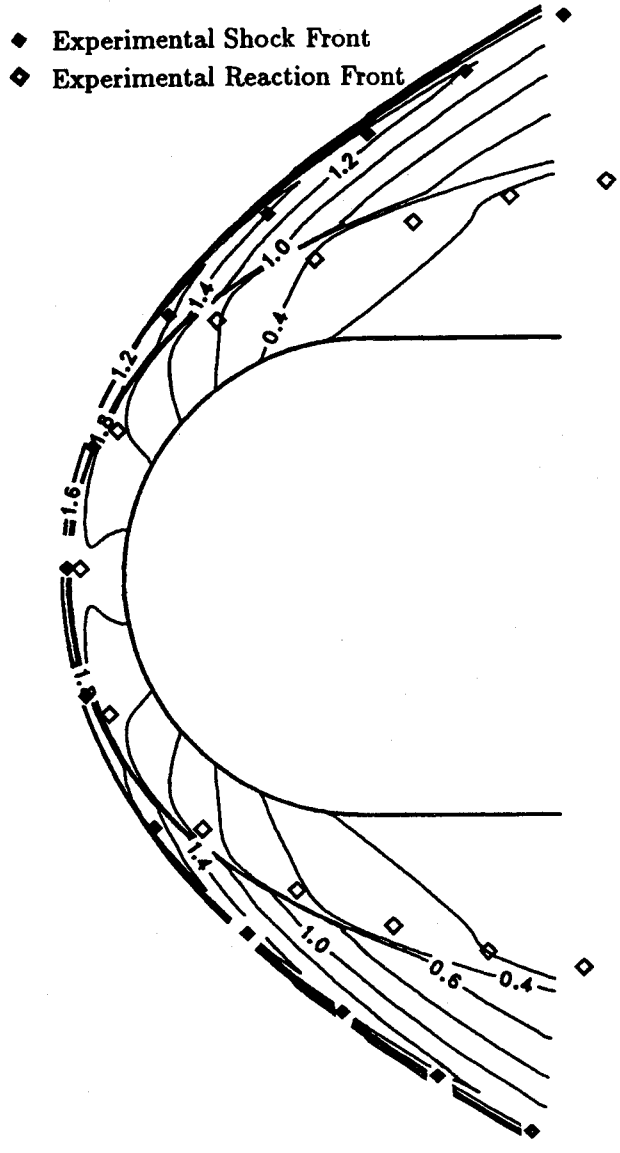

Fig. 6a Comparison of calculated density contours (kg/m^3) with experimental front positions for the Mach 5.11 case.

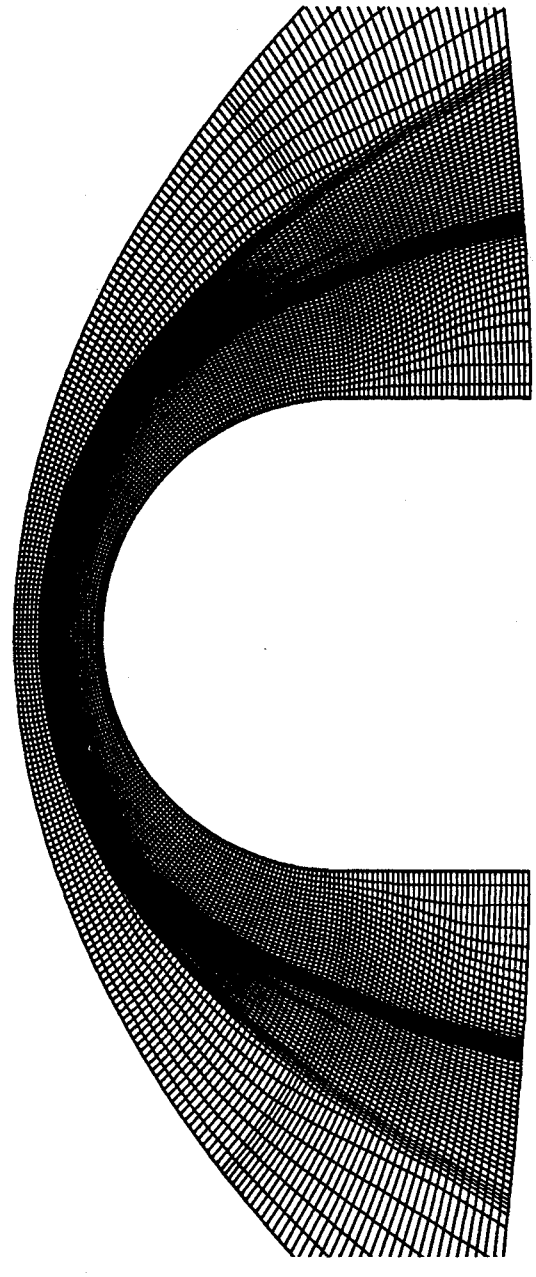

Fig. 6b 127 × 65 adapative mesh used for the calculation presented in Fig. 6a.

each of the following three rate expressions are considered to replace Reaction (2):

$$K_{f2} = 2.60 \times 10^{14} \cdot \exp(-16{,}800/RT) \quad (5a)$$

$$K_{f2} = 1.91 \times 10^{14} \cdot \exp(-16{,}438/RT) \quad (5b)$$

$$K_{f2} = 1.20 \times 10^{17} \cdot T^{-0.91} \cdot \exp(-16{,}513/RT) \quad (5c)$$

Equation (5a) is from Jachimowski's mechanism. Equation (5b) is currently recommended by the National Aerospace Plane Rate Constant Committee.[12] The third rate expression, Eq. (5c), is recommended by Warnatz.[13] All three are similar below 1500 K so that they do not strongly change the mechanism at lower temperatures but they do vary considerably and change the mechanism at higher temperatures. Equation (5a) has the largest values at high temperatures, and Eq. (5c) has the smallest values. Note that smaller values of the rate constant yield longer ignition delay times. The temperature behind the shock for the Mach 5.11 case on the stagnation streamline is approximately 1600 K, which results in a value for K_{f2} of 1.32×10^{12} for Eq. (5a) and 0.808×10^{12} for Eq. (5c) (about 60% of the original one at this temperature). The flowfield calculated using Eq. (5c) is shown in Fig. 7. It shows density contours from the calculation with the shock and reaction front locations digitized from the shadowgraph. The predicted locations are now nearly the same as the experimental ones.

The second approach is to return to the original Jachimowski mechanism and modify Reaction (6) to change the rate at which combustion proceeds after ignition. To do this, the rate expression in Jachimoswki's mechanism

$$K_{f6} = 2.20 \times 10^{22} \cdot T^{-2.0} \quad (6)$$

is reduced by a factor of 4 with the rationale that slowing the rate at which heat is released will reduce the shock-standoff distance (it will be less exothermic). This simple approach is sufficient to test the sensitivity of the flowfield to this reaction. The results show that reducing the Reaction (6) rate constant does not produce flowfield changes as large as the ones seen in Fig. 7. In fact, the changes are difficult to present using a

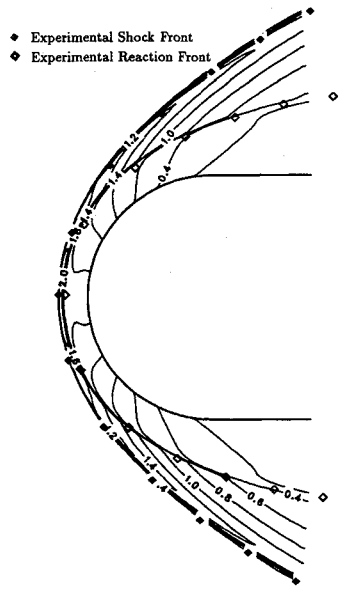

Fig. 7 Density contours (kg/m^3) for the Mach 5.11 case with reaction rate (2) replaced by Eq. (5c).

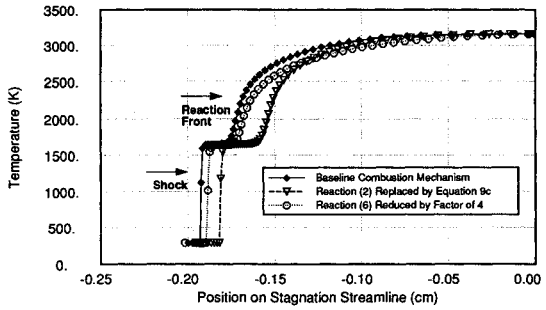

Fig. 8 Temperature profiles along the stagnation streamline for three different reaction sets for the Mach 5.11 case.

contour plot. A clearer picture of the changes are seen by plotting the temperature profile on the stagnation streamline. Figure 8 shows the temperature profile from the original mechanism and the profiles using the new expressions for Reactions (2) and (6). The surface of the projectile is on the right side of the plot at 0.00 cm and the flow is from left to right. It shows that the shock and reaction front locations after reducing the Reaction (6) rate constant are still similar to the original locations. However, close examination shows that the rate constant reduction for Reaction (6) did slow the rate of combustion. It is this profile that approaches the equilibrium value at the wall most slowly.

The third attempt to match the experiment is made by adding freestream water vapor. Rodgers and Schexnayder[14] have discussed the significant effect that freestream water vapor can have on ignition time. To check the influence of water on the Mach 5.11 case, a mole fraction of water equal to 0.02 is added to the freestream. This is a mass fraction equal to 0.017 and represents a relative humidity of about 36% in the ballistic range. The baseline chemistry mechanism is used. The results show that freestream water concentrations move the calculations toward better agreement with experiment. However, it also indicates that the amount of freestream water required to account for the difference between the experiment and the calculation using the baseline chemistry model is probably much greater than existed in the ballistic range.

With the results obtained thus far, it seems logical to use the reaction set with Eq. (5c) as the rate expression for Reaction (2) because it yields the best agreement with experiment. The Mach 6.46 case is calculated with this set. The result is presented in Fig. 9 in the form of density contours overplotted with symbols representing the experimental shock and reaction front positions. Because the Mach number is higher, the temperature behind the shock is higher and the induction zone is significantly thinner than it was in the previous case. It is so small that it appears that the reaction zone is merged with the shock in the stagnation region; however, the adaptive grid places over 10 points between the two fronts. The asymmetry in the experimental front positions indicate that the projectile had a slight angle of attack. Comparing the calculation to the experiment taking this into account shows excellent agreement.

The Mach 6.46 case is a more challenging flowfield calculation than the Mach 5.11 case. One major difference between the two flowfields is that the region where the shock is strong enough to initiate combustion is much larger for the higher Mach number case. This requires a different grid that places more points into induction regions, especially behind the shock in the shoulder region. The new grid curves the normal grid lines so that they become nearly parallel to the streamlines where it is possible to do so (allowing the grid adaptation to be more effective) and also adds more points in the axial direction. Combined, these changes allow more points to be placed along streamlines in the induction zone, which is critical to simulate the flow. The Mach 6.46 grid dimensions are 321 × 65 and it is shown in Ref. 15.

Code Performance

The code runs at 180 MFLOPS on the Numerical Aerodynamic Simulation (NAS) Program's Cray Y-MP at NASA Ames Research Center and takes 8.4 × 10^{-4} s/grid point/iteration. As mentioned in the Numerical Method section, the implicit formulation also leads to high memory requirements. Computations with the 128 × 65 grid required approximately 8 Megawords of memory.

The large equation set is not seen as the primary source of the high computational costs. Instead, the large time requirements are the result of the stiff combustion chemistry and the very small grid spacings required in the induction zone. The small grid spacings reduce the maximum time step and thus require many steps to be taken in order to reach steady state. The small grid spacing also requires that a large number of mesh points must be used. Typical solutions presented here took between 2000 and 4000 iterations and used a maximum Courant-Friedrichs-Lewy (CFL) number of 30. The authors have

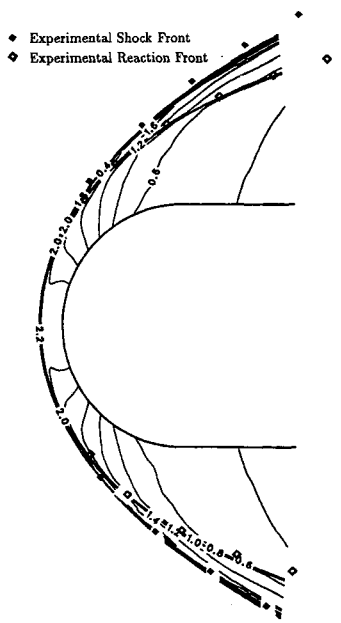

Fig. 9 Comparison of calculated density contours (kg/m^3) with experimental front positions for the Mach 6.46 case.

hope that future work will allow larger time steps to be taken and significantly reduce the iteration requirements.

Conclusions

An axisymmetric, fully implicit, finite volume, computational fluid dynamics code that uses a detailed hydrogen-air combustion mechanism and an adaptive grid has been developed. It is validated using ballistic-range experiments with shock-induced combustion. In these experiments, a 15-mm spherical nose projectile is fired into a premixed hydrogen-air mixture. The separate shock and reaction fronts produced by the blunt body are clearly and accurately captured by the current numerical approach. The ability to do these calculations depends on knowledge gained through numerical studies with quasi-one-dimensional flow, which are used to establish grid requirements for the computations. The studies show that it is critical to have high grid resolution in the induction zone where radical species concentrations increase exponentially. These findings lead us to believe that insufficient grid spacing is the main reason that prior researchers were unable to match the same experimental data.

These simulations have also contributed to the validation of the detailed hydrogen-air combustion mechanism of Jachimowski.[11] Fairly good agreement between the axisymmetric calculations and the ballistic-range experiments is obtained with this mechanism. Better agreement is obtained if the forward rate constant expression for Reaction (2) is replaced by Eq. (5c). Equation (5c) gives a smaller rate constant at high temperatures and thus increases the ignition delay time. There is no conclusive evidence that the new expression for Reaction (2) is, by itself, superior to the original one because a combination of other modifications or effects could account for the same improvements. The change does, however, cause the mechanism to compare more favorably with experiment and it also suggests that some helpful conclusions could be made with more defined data (i.e., by knowing the amount of freestream water vapor or by having more cases under different conditions). In addition, the reaction fronts have been shown to lack sensitivity to the overall combustion speed. This is demonstrated by noting that there are only minor alterations in the shock and reaction front locations when the rate constant for Reaction (6) is modified.

Finally, since the results presented in this paper did not include thermal nonequilibrium effects, it appears that these effects are small for the particular flowfields considered herein. A slightly more detailed discussion of this work can be found in Ref. 15.

Acknowledgments

Funds for the support of this study have been allocated by NASA Langley Research Center and NASA Ames Research Center under the joint research interchange number NCA2-455 and are greatly appreciated. This material is also based on work supported by a National Science Foundation Graduate Fellowship and by NASA under Hypersonic Training and Research Grant NAGW 965. The authors would also like to acknowledge the computer resources provided by NAS and the Aerothermodynamics branch of NASA Ames. The guidance of Richard Jaffe of NASA Ames was invaluable in completing this work and is greatly appreciated. Finally, we are most grateful to H. F. Lehr of the Institute Saint-Louis for providing original photographs of his ballistic-range experiments.

References

[1]MacCormack, R. W., "Current Status of Numerical Solutions of the Navier-Stokes Equations," AIAA Paper 85-0032, Jan. 1985.

[2]Candler, G. V., and MacCormack, R. W., "The Computation of Hypersonic Ionized Flows in Chemical and Thermal Nonequilibrium," AIAA Paper 88-0511, Jan. 1988.

[3]Candler, G. V., "The Computation of Weakly Ionized Hypersonic Flows in Thermo-Chemical Nonequilibrium," Ph.D. Dissertation, Stanford Univ., Stanford, CA, June 1988.

[4]Candler, G. V., "On the Computation of Shock Shapes in Nonequilibrium Hypersonic Flows," AIAA Paper 89-0312, Jan. 1989.

[5]Gökçen, T., "Computation of Hypersonic Low Density Flows with Thermochemical Nonequilibrium," Ph.D. Dissertation, Stanford Univ., Stanford, CA, June 1989.

[6]Lehr, H. F., "Experiments on Shock-Induced Combustion," *Astronautica Acta*, Vol. 17, 1972, pp. 589–596.

[7]Yungster, E., Eberhardt, S., and Bruckner, A. P., "Numerical Simulation of Shock-Induced Combustion Generated by High-Speed Projectiles in Detonable Gas Mixtures," AIAA Paper 89-0673, Jan. 1989.

[8]Lee, S., and Deiwert, G. S., "Calculation of Nonequilibrium Hydrogen-Air Reactions with Implicit Flux Vector Splitting Method," AIAA Paper 89-1700, June 1989.

[9]Stull, D. R., and Prophet, H., "JANAF Thermochemical Tables, 2nd Edition," National Bureau of Standards, National Standard Reference Data Series Rept. 37, June 1971.

[10]Willetts, A., Gaw, J. F., Handy, N. C., and Carter, S., "A Study of the Ground Electronic State of Hydrogen Peroxide," *Journal of Molecular Spectroscopy*, Vol. 135, 1989.

[11]Jachimowski, C. J., "An Analytical Study of the Hydrogen-Air Reaction Mechanism With Application to Scramjet Combustion," NASA TP-2791, Feb. 1988.

[12]Oldenborg, R., Chinitz, W., Friedman, M., Jaffe, R., Jachimowski, C., Rabinowitz, M., and Schott, G., "Hypersonic Combustion Kinetics; Status Report of the Rate Constant Committee, NASP High Speed Propulsion Technology Team," NASP Rate Constant Committee, NASP TM-1107, 1990.

[13]Gardiner, W. C., Jr., *Combustion Chemistry*, Springer-Verlag, New York, 1984.

[14]Rogers, C. R., and Schexnayder, C. J., "Chemical Kinetic Analysis of Hydrogen-Air Ignition and Reaction Times," NASA TP-1856, June 1981.

[15]Wilson, G. J., and MacCormack, R. W., "Modeling Supersonic Combustion Using a Fully-Implicit Numerical Method," AIAA Paper 90-2307, 1990.